REMOVAL PATTERN OF PARTICULATE MATTER FROM CONDENSING HEAT EXCHANGER AFTER WET DESULFURIZATION OF COAL-FIRED UNIT

Shifeng Deng, Qinxin Zhao, Teng Qu, Ning Wang, Huaishuang Shao*

School of Energy and Power Engineering, Xi'an Jiaotong University

*Corresponding author; E-mail: shaohs@xjtu.edu.cn

The flue gas after wet desulfurization of coal-fired units still contains a large amount of particulate matter. Flue gas condensing heat exchangers are often used to further remove particulate matter. However, current research focuses on the overall removal effect of the heat exchangers, but ignores the difference of pollutant removal ability of the inner tube bundle along the flue gas flow direction. This paper studied the correlation between pollutant removal and operating parameters of condensation heat exchanger, so as to make the removed amount of pollutants as large as possible. A field experimental platform was built on a 3×350 MW supercritical circulating fluidized bed coal-fired unit. The total amount of pollutants removed between the 3rd and 6th rows of tube bundles from the inlet of the heat exchanger was the largest. The removal of particulate matter near the outlet of the heat exchanger was the smallest. The highest removal rate of filterable particulate matter (FPM) reached 76 %. The proportion of condensable particulate matter (CPM) in the total removal of particulate matter reached around 90 %. The mass ratio of both H_2SO_4 and SO_3 to the removed CPM were more than 95 %.

Key words: *Flue gas after wet desulfurization; Filterable particulate matter; Condensable particulate matter; Grouped tube bundles; Condensation*

1. Introduction

Coal-fired units generate a large amount of particulate matter (PM) during the combustion process. Although the current dust collector can remove more than 99.6 % of the PM [1], the flue gas still contains a large amount of the PM. The PM is composed of two major categories: filterable particulate matter (FPM) and condensable particulate matter (CPM). The FPM contains a variety of heavy metals [2,3], salts [4], and insoluble minerals [5] etc.; the CPM includes polycyclic aromatic hydrocarbons [6], acid gases [7], soluble salts, which will be transformed into particulate matter when they are condensed. The FPM after electrostatic precipitator is mainly $PM_{2.5}$. $PM_{2.5}$ can penetrate alveolar cells and enter human blood, so it is also known as lung-infiltrating particles. Many scholars have discussed the harm of $PM_{2.5}$ [8,9], which has a carcinogenic risk. Removal of the PM has been a popular research direction in the past decades, which can be divided into two categories: pre-combustion control [10] and post-combustion removal [11]. Pre-combustion control can only reduce the original total amount of particulate matters. Therefore, removal after combustion is necessary.

The original PM in the flue gas is as high as hundreds of mg/m^3 order of magnitude, which can be reduced to several tens of mg/m^3 after passing through the dust collector [12], and can be reduced to

about 10 mg/m^3 order of magnitude after passing through the wet desulfurization tower. The wet desulfurization tower has a significant removal effect on the PM, but it will increase the proportion of $PM_{2.5}$ in the PM [13]. Only a desulfurization tower with efficient mist removal can reduce the content of $PM_{2.5}$ [14]. Low efficient mist removal or too high inlet flue temperature will lead to the evaporation and crystallization of desulfurization slurry, and the mass concentration of PM_1 can be even increased by 59 % [15]. Even if the thermal power unit had completed the ultra-low emission transformation, and the FPM was suppressed to within 5 mg/m^3, the concentration of the CPM was still above 10 mg/m^3.

At present, the research on deep removal of the $PM_{2.5}$ and the CPM mainly focused on the front, inside and rear parts of the wet desulfurization tower, which can be divided into 6 categories: Physical charge agglomeration removal before the desulfurization tower [16]; Spraying steam into desulfurization tower [17]; Spraying chemical agglomeration into desulfurization tower for agglomeration removal [18]; Building a spray tower after the desulfurization tower for washing removal [19]; Building a wet electrostatic precipitator after the desulfurization tower for physical removal [20]; Setting up a condensing heat exchanger after the desulfurization tower for condensation removal [20]. The core of various methods is to agglomerate small-sized particles into large particles that can be trapped and removed. Charged agglomeration can reduce about 50 % of the $PM_{2.5}$ [22], and the addition of chemical coagulant can remove about 30 % of $PM_{2.5}$, up to 65 %. These two methods do not involve a condensation process and focus on removal of filterable $PM_{2.5}$. The spraying vapor condensed on the surface of the particles, which increased the size of the particles. The spray tower is accompanied by the condensation process of water vapor on the surface of the droplets, which can remove 30-80 % of the $PM_{2.5}$ [23,24], and can also remove up to 80 % of SO_3 because of the lower condensation temperature. There is a small amount of condensation process inside wet electrostatic precipitator. The removal rate of SO_3 by wet electrostatic precipitator with different structures ranges from 50 % [25] to 90 % [26], and the PM outlet concentration can be reduced as low as 0.43 mg/m^3 [27]. The PM removal efficiency is even as high as 90% [28], but the SO_3 concentration of some units also increases, which is caused by the oxidation of SO_2 by the electric field [29]. Tan, H. studied the ability of condensing heat exchangers to remove pollutants [30]. There is a strong steam condensation process inside the condensing heat exchanger. The steam condenses on the surface of the PM, which increases the particle size of the PM, and the acid vapor is also condensed below the dew point temperature. A large amount of low-temperature waste heat can be recovered during condensing heat exchanger operation, which can be used for waste heat boiler feed water or as a heat source for heat pumps.

The current research on pollutant removal by condensing heat exchangers mostly focuses on the distribution of particulate matter at the inlet and outlet of the heat exchanger and the composition analysis of the condensed water in the heat exchanger. There are few studies on the removal pattern of pollutants inside the heat exchanger, the condensate composition in different areas, and the scaling and corrosion risks of tube bundles in different areas. Therefore, this paper presents the pollutant removal pattern and condensate water composition in different tube bundle areas of the condensation heat exchanger. The research in this paper can guide the design of condensation heat exchanger, improve its pollutant removal performance, and reduce the corrosion risk during operation.

2. Experimental Section

The test was carried out in a 3 × 350 MW supercritical circulating fluidized bed power plant. As shown in Fig. 1, the test bench was located below a horizontal flue duct from the exit of the #2

limestone-gypsum wet desulfurization tower to the chimney. A hole with a diameter of 400 mm was made in the horizontal flue duct, and a centrifugal fan was used to extract flue gas from the hole to the test bench. The flow rate of the extracted flue gas ranged from 300 m^3/h to 3000 m^3/h. The total flue gas flow rate of the power plant was about 1000000 m^3/h. The system of the test bench included enamel condensing heat exchanger, variable frequency mechanical ventilation cooling tower, circulating water pump, temporary chimney, connecting flue duct, etc. (Fig. 2). Enamel coating improves the corrosion resistance of tube bundle. Enamel condensing heat exchanger, variable frequency mechanical ventilation cooling tower and circulating water pump form a water side circulation loop, and an electromagnetic flowmeter was set on the water side circulation loop to monitor the circulating water flow. Increasing the frequency of the mechanical ventilation cooling tower may reduce the temperature of the circulating water path. The front and rear of the enamel condensing heat exchanger were set with a horizontal flue whose length was 4 times the hydraulic diameter of the flue duct. The temperature measuring points, pressure measuring points, humidity measuring points, and Electrical Low Pressure Impactor (ELPI) exhaust pipe interfaces were arranged on the horizontal flue duct. Temperature measuring points were installed at the inlet and outlet of the enamel condensing heat exchanger of the water side. A vortex flowmeter with temperature and pressure correction was arranged in the middle section of the temporary chimney to measure the flue gas flow. The data of all temperature measurement points, pressure measurement points, and flow measurement points were summarized into the control cabinet, and the control cabinet could control the frequency of each frequency conversion device.

Figure 1. Experimental test platform. ①: horizontal flue ②: chimney ③: enamel condensing heat exchanger ④: ELPI.

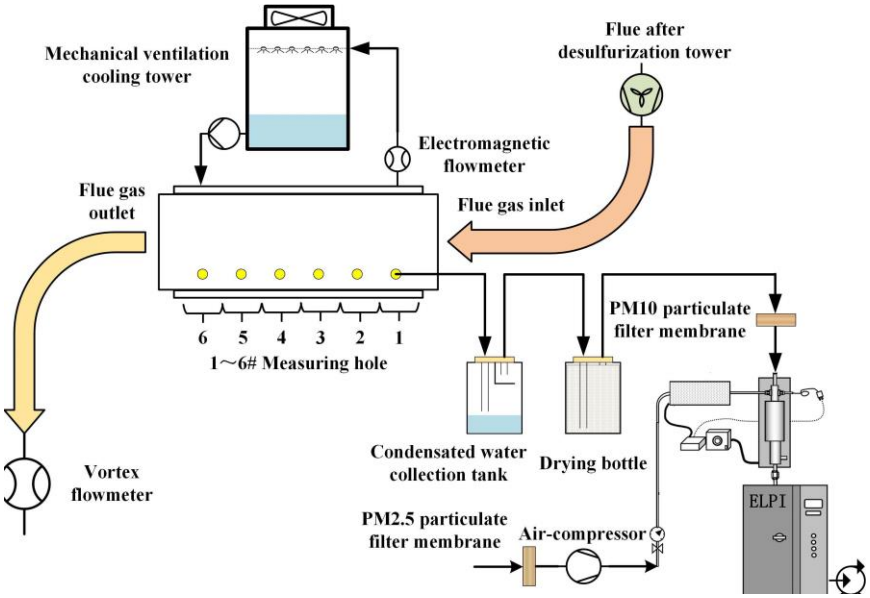

Figure 2. The system diagram of experiment bench.

The testing instrument used in this paper to detect particle size distribution in flue gas is the ELPI produced by DEKATI, Finland, which can detect the mass and quantity concentration of particles with aerodynamic diameter (particle size) between 6 nm and 10 μm in real time. The flue gas after WFGD is wet saturated flue gas, which contains a large number of small droplets. Small droplets will directly enter the ELPI, which will interfere with the test results. Fig. 3 exhibits the constant temperature dilution system, in which the air is preheated to 80 ℃ and then sent to the heat tracing diluter at 60 °C to dilute the wet saturated flue gas to 8 times the original volume. The water dew point of flue gas is lowered to 20 °C. The small droplets carried in the original flue gas are completely evaporated and then sent to the ELPI. The ELPI can record data once per second, and each sampling period is 120 s. When the fluctuation of the maximum and minimum data within 120 s is within 10 %, the average value within the sampling period is taken as the record value. The data measured by the ELPI are distributed in 15 levels, including 15 particle sizes ranging from 0.07 μm to 7 μm.

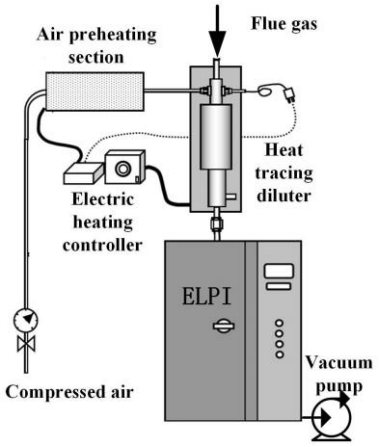

Figure 3. The system diagram of the ELPI.

The enamel plain tubes are placed vertically, the tube diameter of enamel plain tubes is 25 mm, the wall thickness is 2 mm, the number of horizontal rows is 7, the number of vertical rows is 12, transverse pitch is 56 mm, longitudinal pitch is 45 mm. The height of flue gas flow cross-sectional area is 400 mm, the width is 420 mm. The working fluid turns in the water chamber. The enamel pipes of heat

exchanger are divided into 6 areas along the flue gas flow direction. Baffles are arranged along the bottom of the enamel pipe condensing heat exchanger. The width of the baffles is 260 mm, the height is 20 mm, and the thickness is 5 mm, forming a 140 mm wide condensate flow channel. The condensed water flows along the outer wall of the enamel pipe to the bottom of the heat exchanger, and flows to the condensed water flow channel under the restriction of the baffles. Measuring holes are opened on the side of the enamel pipe condensing heat exchanger, and the hoses are used to reach the positions of the 6 five-pointed stars to extract condensed water (Fig. 4a). The location for extracting condensed water is located at the bottom of the heat exchanger, 130 mm away from the condensed water circulation channel to prevent the interference of condensed water in the mainstream area (Fig. 4b).

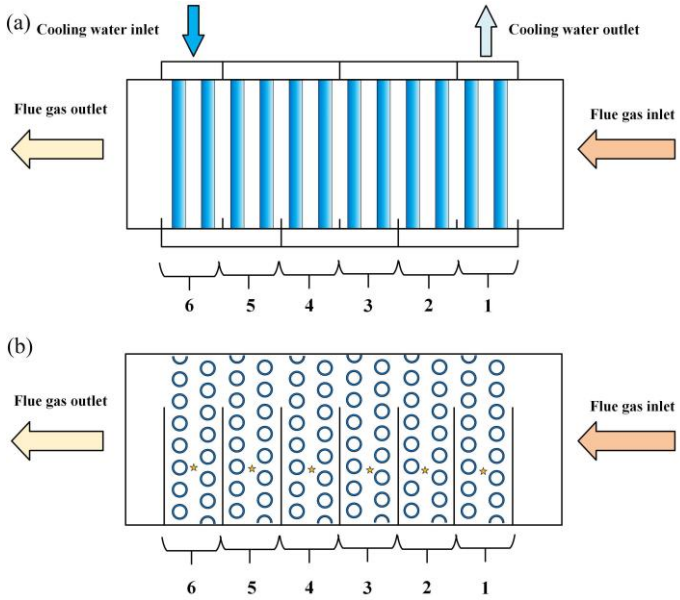

Figure 4. The system diagram of experiment bench. (a) side view of the enamel pipe condensing heat exchanger. (b) cross-sectional top view of the enamel tube condensing heat exchanger

In each set group of experiments, the variable-frequency mechanical ventilation cooling tower and the circulating pump were first turned on, and the frequency was maintained at the maximum, so that the water temperature of the water-side circulating circuit was reduced to the vicinity of the wet bulb temperature corresponding to the current atmospheric conditions. After the temperature of the water side was stable, the variable frequency centrifugal fan is turned on, and the frequency of the variable frequency centrifugal fan was adjusted to maintain the flue gas volume at the predetermined test flue gas volume. After the inlet and outlet flue gas and water temperatures of the tested condensing heat exchanger were stable, the ELPI system was connected to 6 measurement points to measure the quantity concentration and mass concentration of particulate matter. And the flue gas temperature, water chamber temperature, and other parameters were recorded. The mixture of condensed water and flue gas extracted from 6 measurement points was separated and stored in the condensed water collection tank. The frequency of the variable frequency centrifugal fan and the variable frequency mechanical ventilation cooling tower was changed to obtain the working conditions of different flue gas flow and cooling water temperature.

3. Results and discussions

During the experiment, the condensed water was collected. The condensed water formed by the condensation of water vapor does not contain ionic components, so the ionic components detected in the condensed water were all derived from the pollutants removed from the flue gas. Given the condensed water flow rate, the ion composition and total amount in the condensed water, the total mass of pollutants removed during the condensation process could be calculated. The removal mass of filterable particulate matter in flue gas could be measured by the ELPI. The removed pollutants were composed of three parts: FPM, CPM, and ions carried by the escaping desulfurization slurry [31]. After passing through the mist eliminator on the top of the desulfurization tower, the flue gas carried about 75 mg/m^3 of desulfurization slurry. The composition analysis of desulfurization slurry is shown in Tab. 1, the particle size of the escaped desulfurization slurry droplets was usually less than 2.5 μm, and the removal pattern was similar to that of the FPM. Therefore, it was assumed that the removal rate of the FPM in each area was the same as that of the escaped desulfurization slurry. When the total amount of pollutants was removed, the removal of the FPM and the removal of ions carried by the escaped desulfurization slurry was calculated, as well as the semi-quantitative calculation of the removal of the CPM in each tube bundle area.

Tab. 1. Composition analysis of desulfurization slurry in desulfurization tower

Concentration	Cl^-	NO_3^-	SO_4^{2-}	Ca^{2+}	Mg^{2+}	K^+	Na^+	TDS
mg/L	251.8	118.7	3205.9	1318.9	109.1	17.8	7.0	5105

In general, with the decrease of cooling water temperature, the removal rate of particles gradually increased (Fig. 5). Although the total amount of pollutants removed has been changing, the removal pattern of particulate matter in condensing heat exchanger generally shows a trend of increasing first and then decreasing. The area #1 was at the inlet of the heat exchanger where the flue gas between the tube bundles has not yet cooled down, and the volume of the supercooled area of the flue gas was less than that of the area #2, so the removal of particulate matter was less than that of the area #2. The concentration of particulate matter in areas #3 to #6 continued to decrease, so the amount of removal also decreased.

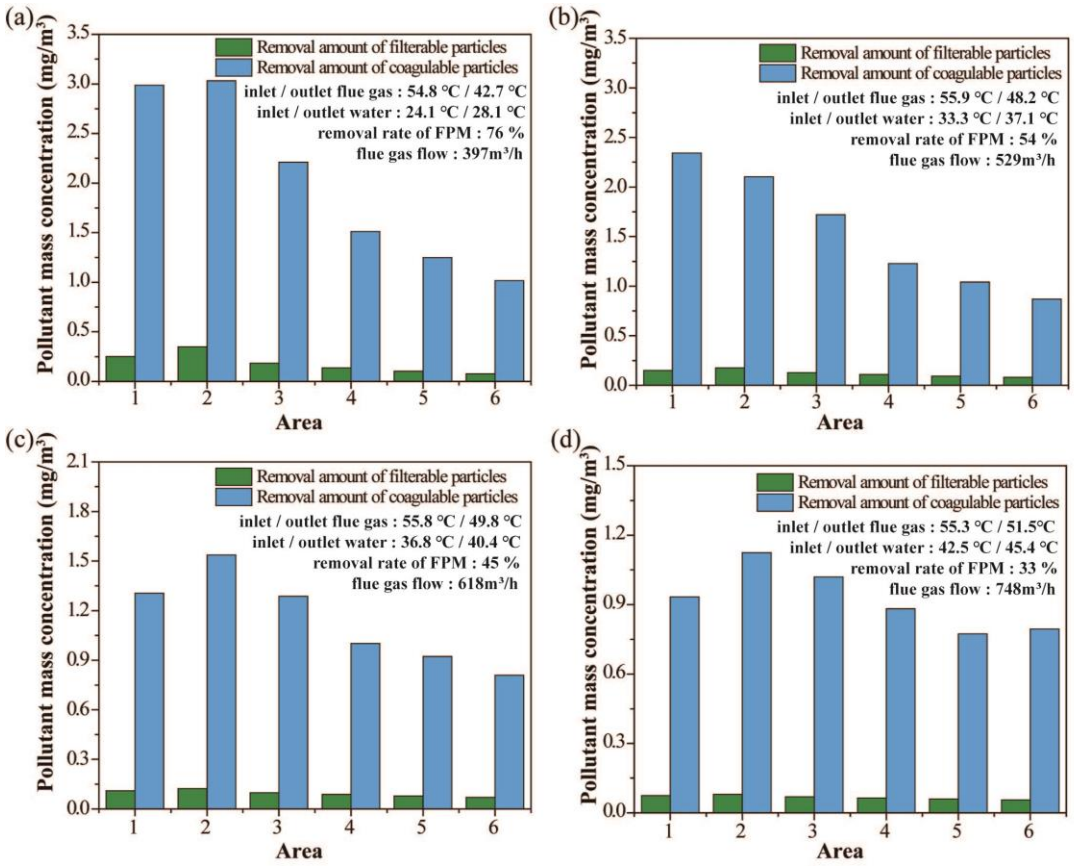

Figure 5. Removal of pollutants in each area under four working conditions.

Taking the working condition in Fig. 5a as an example, the composition analysis of various anions is shown in Tab. 2. The pH represents the concentration of H^+. The anion concentration and pH in the condensed water determined the strength of the condensed water's corrosion performance. The pH first decreased and then increased, and the lowest pH was located in the area #4. The pH of the desulfurization slurry was about 5.5, and the pH of the condensed water was significantly lower than that of the desulfurization slurry. From the analysis of the composition of anions, the main reason for this phenomenon was the condensation of SO_3/H_2SO_4. SO_3/H_2SO_4 which exits in the form of aerosol with a particle size of less than 1 μm in the flue gas after the desulfurization tower, which continuously absorbed water vapor in the condensing heat exchanger, resulting in continuous increase in size. When the size was greater than 2.5 μm, it could be effectively captured and removed. The #1 area acted as a particle agglomerator, which significantly increased the SO_3/H_2SO_4 particle size in the flue gas. Therefore, the area with the largest SO_3/H_2SO_4 capture was the area #2~4 of the heat exchanger. After the area #4, the total amount of SO_3/H_2SO_4 decreased, so the capture rate in a single interval decreased. The mass ratio of SO_3/H_2SO_4 to the removed CPM was more than 95 %. The concentrations of other anions apart from SO_4^{2-} were lower. The concentrations of all anions showed a trend of first increasing and then decreasing.

Table 2. Ionic composition analysis of condensate in each area of Fig. 5a

Concentration mg/L	Cl^-	SO_4^{2-}	NO_3^-	NO_2^-	F^-	pH
#1	0.58	97.47	0.62	0.43	0.44	2.72
#2	0.72	112.9	0.72	0.44	0.72	2.72
#3	0.35	85.51	0.62	0.51	0.32	2.45
#4	0.41	65.73	0.96	0.41	0.31	2.36
#5	0.6	58.52	0.55	0.34	0.24	2.54
#6	0.32	52.95	0.37	0.36	0.2	2.45

Tab. 3 was the analysis of the anion composition of the corresponding working conditions in Fig. 5d. From the area #1 to #6, the pH first decreased, then increased and finally remained unchanged. The pH of the area #2 was the lowest; the ion concentration first increased and then decreased, and the area #2 had the lowest pH. The temperature of the circulating cooling water in Fig. 5d was higher, and the amount of condensed water was less, so the ion concentration in the condensate was higher.

Table 3. Ionic composition analysis of condensate in each area of Fig. 5d

Concentration mg/L	Cl^-	SO_4^{2-}	NO_3^-	NO_2^-	F^-	pH
#1	0.34	128.3	0.7	0.62	0.8	2.36
#2	0.4	143.3	0.8	0.68	0.83	2.18
#3	0.63	132.6	0.7	0.51	0.7	2.36
#4	0.32	128.2	0.65	0.6	0.32	2.63
#5	0.3	121.3	0.55	0.45	0.64	2.63
#6	0.31	120.2	0.55	0.62	0.29	2.65

Under the working conditions shown in Fig. 5a, the particles of each particle size were in the dynamic equilibrium of generation and removal. Particles with a particle size of 0.02 μm to 0.13 μm were generated in large quantities in the first half of the condensing heat exchanger, and the concentration was even higher than the original flue gas, which meant that a large number of particles with a particle size smaller than 0.02 μm were removed in the first half of the condensing heat exchanger. The removal rate of particles with a particle size greater than 0.2 μm in the heat exchanger was greater than the generation rate, and the particle concentration continues to decrease with the condensation of water vapor in the flue gas. Particles with a particle size larger than 2.5 μm mainly relied on the collision capture of the enamel tube bundles, and begin to be removed in large quantities when they enter the condensing heat exchanger.

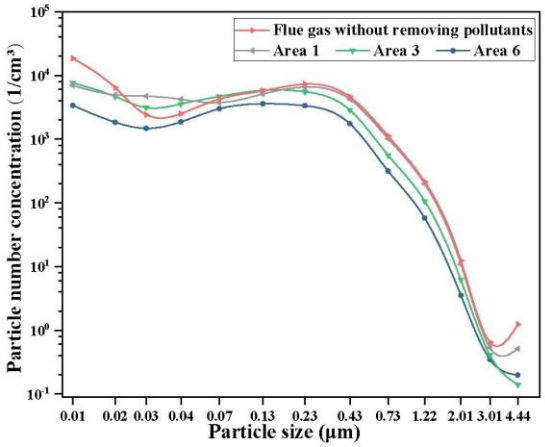

Figure 6. Concentration of filterable particles in three areas of Fig. 5a

The core method of particle removal was to make the particle size greater than 2.5 μm, and the particle size greater than 2.5 μm was easy to be captured by the heat exchanger wall. The condensation of water vapor on the surface of the particulate matter could increase the particle size, and the small droplets formed by the condensation of water vapor could collide with the particulate matter to form larger particulate matter. Both of these processes that increased the particle size of particulate matter relied on water vapor condensing inside the flue gas rather than condensing on the heat exchanger surface. Based on the classical nucleation theory, the competitive relationship between the chemical potential energy and the surface energy of water determined the critical nucleation work and the steady-state nucleation rate. According to the different position of water vapor condensation, it could be divided into homogeneous nucleation and heterogeneous nucleation [32]. Homogeneous nucleation is the formation of liquid droplets inside water vapor as the condensation nucleus of water vapor, while heterogeneous nucleation is the condensation of water vapor on the existing solid surface. The ratio of heterogeneous nucleation rate J_{het} to homogeneous nucleation rate J_{hom} could be obtained from Equ. 2. The maximum supersaturation degree S is defined to reflect the effect of supersaturation on the removal of filterable particulate matter, $S=P_{sat}/P_s$. P_{sat} is the saturation pressure corresponding to the average water dew point of the flue gas, and P_s is the saturation pressure corresponding to the average cooling water temperature. When the surface energy of water remains unchanged, with the increase of S, the chemical potential difference before and after the phase transition increases, and the proportion of homogeneous nucleation in the condensation process increases. As shown in Fig. 7, with the increase of S, the main condensation process gradually transfers from the enamel surface to the particle surface, and S in the experimental conditions does not increase to the magnitude of saturation dominated by homogeneous nucleation. When water vapor condenses on the surface of particles, it promotes the increase of particle size. Particles and water droplets collide with each other and condense into larger particles to be captured and removed by the enamel surface.

$$\frac{J_{het}}{J_{hom}} = 10^{-7} \frac{\alpha(\theta)}{\sqrt{f(\theta)}} \exp\left[\frac{W^*}{k_B}(1-f(\theta))\right] \tag{2}$$

Where k_B is the Boltzmann constant, 1.38*10^-23J/K; T is the average flue gas temperature , K; $W^* = 16\sigma^3 \bar{v}^2 / \left[3*(\Delta\mu)^2\right]$ is the homogeneous critical nucleation work, J; $\alpha(\theta) = (1-\cos(\theta))/2$ is the shape factor; $f(\theta) = (2-3\cos(\theta)+\cos^2(\theta))/4$ is the catalytic factor; σ is the surface tension of water, N/m^2; $\bar{v}$ is the average molecular of water, m^3; $\Delta\mu = -k_B T \ln(S)$ is the change of chemical potential during phase transition, J; θ is the contact angle of water on enamel surface.

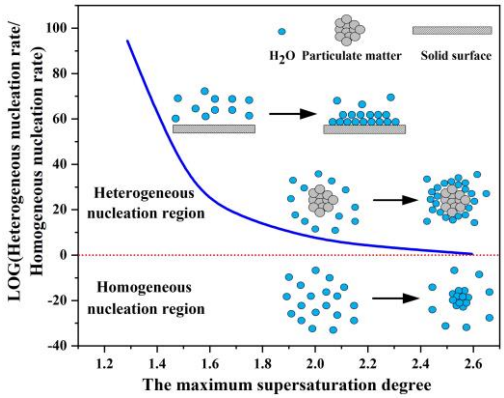

Figure 7. The ratio of heterogeneous nucleation rate to homogeneous nucleation rate varies with maximum supersaturation degree

The *S* from the flue gas inlet to the flue gas outlet of the heat exchanger decreased from about 2 to about 1.2. Heterogeneous nucleation dominated the condensation process under test conditions. After the flue gas entered the condensation heat exchanger, the saturated water vapor and partial CPM began to condense on the surface of tube bundles and the PM. Condensate film appeared on the surface of the tube bundles to capture $PM_{3\sim10}$. Water vapor and partial CPM generated a large number of small droplets and $PM_{0.03}$ with $PM_{0.01}$ as the core. A small part of water vapor and the CPM generated liquid droplets and $PM_{0.03}$ by homogeneous nucleation. Liquid droplets, CPM and $PM_{0.03}$ collided together to generate a large number of $PM_{0.2}$. Phase change aggregation and removal of $PM_{3\sim10}$ were the main components in area #1. With the continuous condensation, a large amount of PM_3 and the CPM are converted into $PM_{3\sim10}$, which is removed by tube bundles in areas #2 and #3. The total amount of the PM_3 and CPM in areas #4, #5 and #6 decreased gradually, therefore the $PM_{3\sim10}$ removed in the tube bundles was also gradually decreasing. The generation rate of $PM_{0.3}$ in areas #4, #5 and #6 was less than the removal rate, so the amount of $PM_{0.3}$ began to decrease. The flue gas condensation process was accompanied by the collaborative removal of the FPM and CPM (Fig.8).

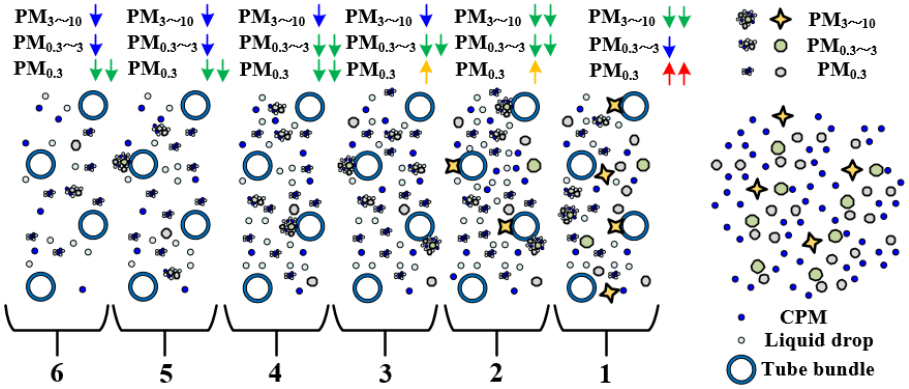

Figure 8. Analysis of PM removal process

4. Conclusions

In this study, the flue gas and condensate water in each tube bundle area of the heat exchanger from the inlet to the outlet was analyzed. According to the above analysis, the patterns of the removal of pollutants are deduced as follows:

The removal of pollutants in the heat exchanger showed a trend of firstly increasing and subsequently decreasing. The total amount of pollutants removed between the 3rd and 6th rows of tube bundles from the inlet of the heat exchanger was the largest, and the amount of pollutants removed at the outlet of the heat exchanger was the smallest.

The total pollutants removal rate was related to the cooling water temperature of the heat exchanger. As the temperature of cooling water decreased, the amount of pollutants removal gradually increased. The highest removal rate of the FPM reached up to 76 %.

During operation, the condensed water near the inlet of the heat exchanger is most corrosive, pH of condensed water is only 2 to 3. The proportion of the CPM in the total removal of pollutants could reach about 90%. The main components of the CPM in coal-fired power plants are SO_3/H_2SO_4.

Acknowledgments

This research was supported by the National Natural Science Foundation of China (51876165) and the Key Research and Development Program of Shaanxi Province (2021GXLH-Z-005), which are gratefully acknowledged.

References

[1] Xu, Y., et al., Field Measurements on the Emission and Removal of PM2.5 from Coal-Fired Power Stations: 3. Direct Comparison on the PM Removal Efficiency of Electrostatic Precipitators and Fabric Filters, Energy & Fuels, 30. (2016), 7, pp. 5930-5936, DOI No. 10.1021/acs.energyfuels.6b00425
[2] Goodarzi, F.,H. Sanei, Plerosphere and its role in reduction of emitted fine fly ash particles from pulverized coal-fired power plants, Fuel, 88. (2009), 2, pp. 382-386, DOI No. 10.1016/j.fuel.2008.08.015
[3] Zhao, S., et al., Migration Behavior of Trace Elements at a Coal-Fired Power Plant with Different Boiler Loads, Energy & Fuels, 31. (2016), 1, pp. 747-754, DOI No. 10.1021/acs.energyfuels.6b02393
[4] Hu, Z., et al., Emission characteristics of particulate matters from a 30 MW biomass-fired power plant in China, Renewable Energy, 155. (2020), pp. 225-236, DOI No. 10.1016/j.renene.2020.03.094
[5] Zhao, Y., et al., Establishment of a database of emission factors for atmospheric pollutants from Chinese coal-fired power plants, Atmospheric Environment, 44. (2010), 12, pp. 1515-1523, DOI No. 10.1016/j.atmosenv.2010.01.017
[6] Kong, S., et al., Emission and profile characteristic of polycyclic aromatic hydrocarbons in PM2.5 and PM10 from stationary sources based on dilution sampling, Atmospheric Environment, 77. (2013), pp. 155-165, DOI No. 10.1016/j.atmosenv.2013.04.073
[7] Wang, X., et al., Experimental and kinetics study on SO3 catalytic formation by Fe2O3 in oxy-combustion, J Environ Manage, 236. (2019), pp. 420-427, DOI No. 10.1016/j.jenvman.2019.02.007
[8] Goodarzi, F., The rates of emissions of fine particles from some Canadian coal-fired power plants, Fuel, 85. (2006), 4, pp. 425-433, DOI No. 10.1016/j.fuel.2005.07.008
[9] Nielsen, M.T., et al., Formation and emission of fine particles from two coal-fired power plants, Combustion Science and Technology, 174. (2002), 2, pp. 79-113, DOI No. 10.1080/714922606
[10] Kazagic, A., et al., Selection of sustainable technologies for combustion of Bosnian coals, Thermal Science, 14. (2010), 3, pp. 715-727, DOI No. 10.2298/tsci1003715k
[11] Lu, J.,X. Ren, Analysis and discussion on formation and control of primary particulate matter generated from coal-fired power plants, J Air Waste Manag Assoc, 64. (2014), 12, pp. 1342-51, DOI No. 10.1080/10962247.2014.951744
[12] Eric, M., et al., Results of the modernization of the electrostatic precipitator at unit B1 of the Thermal Power Plant Kostolac B, Thermal Science, 22. (2018), Suppl. 5, pp. 1623-1634, DOI No. 10.2298/tsci18s5623e
[13] Yao, S., et al., Effect of wet flue gas desulfurization (WFGD) on fine particle (PM2.5) emission from coal-fired boilers, J Environ Sci (China), 77. (2019), pp. 32-42, DOI No. 10.1016/j.jes.2018.05.005
[14] Liu, X., et al., Field Measurements on the Emission and Removal of PM2.5 from Coal-Fired Power Stations: 1. Case Study for a 1000 MW Ultrasupercritical Utility Boiler, Energy & Fuels, 30. (2016), 8, pp. 6547-6554, DOI No. 10.1021/acs.energyfuels.6b00423
[15] Ruan, R., et al., Effects of APCDs on PM emission: A case study of a 660 MW coal-fired unit with ultralow pollutants emission, Applied Thermal Engineering, 155. (2019), pp. 418-427, DOI No. 10.1016/j.applthermaleng.2019.03.136

[16] Chen, D., et al., Experimental investigation of aerodynamic agglomeration of fine ash particles from a 330 MW PC-fired boiler, Fuel, 165. (2016), pp. 86-93, DOI No. 10.1016/j.fuel.2015.10.036
[17] Liu, H., et al., Experimental investigation on a novel agglomeration device based on charged ultrasonic spray and vortex generators for improving the removal of fine particles, Fuel, 287. (2021), DOI No. 10.1016/j.fuel.2020.119549
[18] Lei, Z., et al., Improving the removal of fine particles by chemical agglomeration during the limestone-gypsum wet flue gas desulfurization process, Journal of Environment Science, 80 (2019), pp.37-46, DOI No. 10.1016/j.jes.2018.07.013
[19] Yang, F., et al., Effects of Wet Flue Gas Desulfurization and Wet Electrostatic Precipitator on Particulate Matter and Sulfur Oxide Emission in Coal-Fired Power Plants, Energy & Fuels, 34. (2020), 12, pp. 16423-16432, DOI No. 10.1021/acs.energyfuels.0c03222
[20] Wang, K., et al., Characteristics of condensable particulate matter before and after wet flue gas desulfurization and wet electrostatic precipitator from ultra-low emission coal-fired power plants in China, Fuel, 278. (2020), DOI No. 10.1016/j.fuel.2020.118206
[21] Cao, R., et al., Condensational growth activated by cooling method for multi-objective treatment of desulfurized flue gas: A full-scale study, Chemical Engineering Journal, 410. (2021), DOI No. 10.1016/j.cej.2020.128296
[22] Wang, W., et al., A simple moment model to study the effect of diffusion on the coagulation of nanoparticles due to Brownian motion in the free molecule regime, Thermal Science, 16. (2012), 5, pp. 1331-1338, DOI No. 10.2298/tsci1205331w
[23] Chen, Z., et al., The synergetic particles collection in three different wet flue gas desulfurization towers: A pilot-scale experimental investigation, Fuel Processing Technology, 179. (2018), pp. 344-350, DOI No. 10.1016/j.fuproc.2018.07.025
[24] Darbandi, T., et al., CFD modeling of the forces in the wet scrubber acting on particulate matter released from biomass combustion, Thermal Science and Engineering Progress, 25. (2021), DOI No. 10.1016/j.tsep.2021.100997
[25] Yang, Z., et al., Challenge of SO 3 removal by wet electrostatic precipitator under simulated flue gas with high SO 3 concentration, Fuel, 217. (2018), pp. 597-604, DOI No. 10.1016/j.fuel.2017.12.125
[26] Zheng, C., et al., Formation, transformation, measurement, and control of SO3 in coal-fired power plants, Fuel, 241. (2019), pp. 327-346, DOI No. 10.1016/j.fuel.2018.12.039
[27] Yang, Z., et al., A combined wet electrostatic precipitator for efficiently eliminating fine particle penetration, Fuel Processing Technology, 180. (2018), pp. 122-129, DOI No. 10.1016/j.fuproc.2018.08.013
[28] Kim, H.J., et al., Fine particle removal performance of a two-stage wet electrostatic precipitator using a nonmetallic pre-charger, J Air Waste Manag Assoc, 61. (2011), 12, pp. 1334-43, DOI No. 10.1080/10473289.2011.603994
[29] Anderlohr, C., et al., Collection and Generation of Sulfuric Acid Aerosols in a Wet Electrostatic Precipitator, Aerosol Science and Technology, 49. (2015), 3, pp. 144-151, DOI No. 10.1080/02786826.2015.1008624
[30] Tan, H., et al., Development of wet phase transition agglomerator for multi-pollutant synergistic removal, Applied Thermal Engineering, 130. (2018), pp. 1208-1214, DOI No. 10.1016/j.applthermaleng.2017.11.112
[31] Cheng, T., et al., Emission Characteristics of Soluble Ions in Fine Particulates in Limestone–Gypsum Wet Flue Gas Desulfurization System, Energy & Fuels, 34. (2020), 3, pp. 3836-3842, DOI No. 10.1021/acs.energyfuels.9b04512
[32] Preining, O.， et al., Heterogeneous nucleation and droplet growth, University of Vienna, Vienna, Austria, 1981

Submitted: 22.04.2023
Revised: 25.05.2023
Accepted: 12.06.2023